Journal of King Saud University - Science 35 (2023) 102933

HOSTED BY

Contents lists available at ScienceDirect

Journal of King Saud University - Science

journal homepage: www.sciencedirect.com

Original article

The effect of red betel (*Piper crocatum*) water fraction as tyrosinase inhibitors: In vitro, molecular docking, and molecular dynamics studies

Mega Safithri [a,b,*], Dimas Andrianto [a], Adzani Gaisani Arda [c,h,1], Putri Hawa Syaifie [c,*], Nofa Mardia Ningsih Kaswati [c], Etik Mardliyati [d,*], Donny Ramadhan [e], Muhammad Miftah Jauhar [c], Dwi Wahyu Nugroho [c], Dewi Anggraini Septaningsih [f], Leni Tria Melati [b], Martini Hudayanti [a], Eliwati Sarah [a], Riyan Alifibi Putera Irsal [a], Nurul Taufiqu Rochman [g]

[a] *Department of Biochemistry, Faculty of Mathematics and Natural Science, Bogor Agricultural University, Dramaga Campus, Bogor 16680, Indonesia*
[b] *Tropical Biopharmaca Research Center (Biopharmaca), Institute for Research and Community Service, IPB University, Bogor, Indonesia*
[c] *Nano Center Indonesia, Jl. Raya PUSPIPTEK, South Tangerang, Banten, 15314, Indonesia*
[d] *Research Center for Vaccine and Drug, National Research and Innovation Agency (BRIN), Cibinong Science Center, West Java, 16911, Indonesia*
[e] *Research Center for Pharmaceutical Ingredients and Traditional Medicine, National Research and Innovation Agency (BRIN), Cibinong Science Center, West Java, 16911, Indonesia*
[f] *Advanced Research Laboratory, Bogor Agricultural University, Darmaga Campus, Bogor 16680, Indonesia*
[g] *Research Center for Advanced Material, National Research and Innovation Agency (BRIN), PUSPIPTEK, South Tangerang, Banten, 15314, Indonesia*
[h] *Department of Biochemistry and Molecular Biology, Faculty of Medicine, University of Debrecen, Debrecen H-4032, Hungary*

ARTICLE INFO

Keywords:
In silico
In vitro
Pigmentation
Molecular docking
Molecular dynamics
Red betel

ABSTRACT

Objective: Excessive melanin expression can lead to dermatological conditions such as Riehl melanosis, lentigo, freckles, and melasma post-inflammatory hyperpigmentation. Targeting melanogenesis, the synthesis of melanin, and inhibiting tyrosinase have been explored to mitigate its effects. However, many existing anti-melanogenic agents exhibit severe adverse side effects, necessitating searching for alternative options. In this study, we aimed to investigate the anti-tyrosinase activity of red betel leaves and identify bioactive compounds responsible for their inhibitory effects.

Methods: A 70% ethanol extract of red betel leaves, and its fractions (n-hexane, ethyl acetate, and water) were evaluated for their anti-tyrosinase activity. The inhibitory concentration (IC_{50}) was measured using mushroom tyrosinase as the target enzyme. Subsequently, the bioactive compounds in the water fraction were identified through ultra-high-performance liquid chromatography (UHPLC) analysis. Computational docking analysis was performed on the identified compounds to assess their inhibitory potential against tyrosinase. Additionally, ADMET and molecular dynamics analysis were also performed.

Results: The water fraction of the red betel leaf extract exhibited the most robust anti-tyrosinase activity, with an IC_{50} value of 6.344 ppm. UHPLC analysis of the water fraction revealed the presence of several compounds. Among these, piperine, piperamide-C7:2 (2E,6E), and trichostachine exhibited intense inhibitory activity against tyrosinase, with docking scores of −7.04, −6.87, and −6.79 kcal/mol, respectively. Importantly, all three compounds complied with Lipinski's rules and were classified as non-toxic. Molecular dynamics simulations demonstrated that piperine displayed minimal fluctuation throughout the simulation, as indicated by root mean square deviation (RMSD) and root mean square fluctuation (RMSF) analysis.

Conclusions: Red betel leaves, particularly the water fraction, possess anti-melanogenesis activities. Piperine, piperamide-C7:2 (2E,6E), and trichostachine were identified as critical bioactive compounds responsible for the observed inhibitory effects on tyrosinase. These compounds exhibit solid inhibitory activity without violating Lipinski's rules or posing toxic risks. Furthermore, molecular dynamics simulations suggest the stability of

* Corresponding author at: Department of Biochemistry, Faculty of Mathematics and Natural Science, Bogor Agricultural University, Dramaga Campus, Bogor 16680, Indonesia (Mega Safithri); Nano Center Indonesia, Jl. Raya PUSPIPTEK, South Tangerang, Banten, 15314, Indonesia (Putri Hawa Syaifie); Research Center for Vaccine and Drugs, National Research and Innovation Agency (BRIN), Cibinong Science Center, West Java, 16911, Indonesia (Etik Mardliyati).
E-mail addresses: safithri@apps.ipb.ac.id (M. Safithri), putri@nano.or.id (P. Hawa Syaifie), etik002@brin.go.id (E. Mardliyati).
[1] This author contributed equally to the first author.

https://doi.org/10.1016/j.jksus.2023.102933
Received 7 September 2022; Received in revised form 6 July 2023; Accepted 5 October 2023
Available online 12 October 2023

piperine during the simulation. These findings highlight the potential of red betel leaves as a promising ingredient in the pharmaceutical and cosmetic industries for combating excessive melanin production.

1. Introduction

Melanin is a natural pigment substance that widely occurs in a range of living organisms, including bacteria, fungi, plants, and animals (Costa et al., 2015). It is responsible for the color of skin, hair, and iris and is also a protector against DNA destruction by shielding the nucleus from ultraviolet light (Miller and Zachary, 2017). Melanogenesis, the process of melanin synthesis, is initiated by tyrosinase. A copper-containing binuclear enzyme that converts L-tyrosinase to 3,4-dihydroxyphenylalanine (L-DOPA) is then oxidized to produce dopaquinone (Slominski et al., 2012). Dopaquinone then undergoes further oxidation and several nonenzymatic polymeric reactions to form melanin.

However, the excessive expression of melanin can result in several dermatological conditions such as Riehl melanosis, lentigo, freckles, and melasma post-inflammatory hyperpigmentation (Ball Arefiev and Hantash, 2012; Chandra et al., 2012; Mradula and Sacchidanand, 2012; Xu et al., 2018). Since the role of tyrosinase in melanin production necessitates its impact as a target molecule to minimize the effect of melanogenesis, several agents, such as tyrosinase inhibitors, have been developed.

The mechanisms employed by inhibitors display considerable variation. The investigation of specific tyrosinase inhibitors or mechanism-based inhibitors holds great significance in the realm of pharmacology, particularly concerning the process of hyperpigmentation. It is plausible that the inactivation of tyrosinase occurs due to conformational changes instigated by the substrate, subsequently influencing the solvent molecules in the tertiary and quarternary structures of the enzyme. Additionally, tyrosinase can be inhibited through competitive, uncompetitive, mixed-type (competitive and uncompetitive), and non-competitive means. In the case of competitive inhibition, an inhibitor can bind to an unoccupied enzyme, obstructing substrate binding at the active site. On the other hand, an uncompetitive inhibitor exclusively attaches itself to the enzyme-substrate complex, while a mixed (competitive and uncompetitive) inhibitor can bind to both free enzyme molecules and enzyme-substrate complexes. Conversely, non-competitive inhibitors form bonds with both free enzymes and enzyme-substrate complexes, maintaining an equivalent equilibrium constant (Zolghadri et al., 2019).

Numerous compounds, such as kojic acid, arbutin, and hydroquinone, are well-recognized for their tyrosinase-inhibitory properties. Even these compounds have been used for cosmetic applications to treat hyperpigmentation. However, these drugs are also linked to their severe adverse effects, which include irreversible pigmentation, paradoxical hyperpigmentation, and contact dermatitis (Ando et al., 2010; Ebanks et al., 2009). Therefore, it is necessary to look for alternative anti-melanogenic drugs.

Medicinal plants have been widely employed as active components in therapeutic, cosmetic products, as well as therapies for dermatological conditions like hyperpigmentation, acne, and photoaging. These plants offered untapped sources of potential for the development of active compounds for cosmetic formulations. One of the potential therapeutic herbs used is red betel (*Piper crocatum*) leaf.

Red betel leaves contain active compounds such as alkaloids, tannins, flavonoids, and essential oils (Irawan and Foliatini, 2017; Safithri and Kurniawati, 2016). It has antioxidant activity with an IC_{50} value of 13,5 μg/mL (Septiani, 2017). Fatima et al. revealed in a preliminary study that red betel leaf extract and fractions suppress malondialdehyde (MDA) production, a sign of oxidative stress (Zaelani, Bella Fatima Dora., Safithri, Mega., Adrianto, 2021). It has been demonstrated that the ethyl acetate fraction of red betel can reduce MDA production by up to 79.83%. A high level of MDA in plasma indicates an increase in the generation of free radicals and a decrease in antioxidant levels. By utilizing antioxidants, oxidative stress can be prevented effectively.

Extract and fraction of red betel leaves exhibited tyrosinase-inhibiting activity, as described by Weni, 2015 (Safithri, Mega., Syaefudin, Weni, 2015). The results demonstrated that ethanol extract and n-hexane fraction inhibit tyrosinase more effectively than the other fractions. However, the IC_{50} of red betel extract and fractions as a tyrosinase inhibitor, as well as the interaction of the associated compounds, have not been investigated. We intend to examine the tyrosinase inhibitory activity of red betel leaves in its extract and fractions along with the IC_{50} profiling. As well as the characterization of the active compounds with UHPLC, followed by in silico studies using molecular docking and molecular dynamics modeling, to further investigate compounds that have a role in the anti-melanogenic activity.

2. Materials and method

2.1. Chemicals

Ethanol 70% (Merck), n-hexane (EMSURE), ethyl acetate (Merck), distilled water, dimethyl sulfoxide DMSO), L-DOPA, and tyrosinase. Oven, analytical scale, desiccator, rotary evaporator (110 s-WD Eyela), micropipette (Thermo Scientific), sonicator (BRANSON).

2.2. Preparation, extraction, and fractionation of red betel leaves

The simplicial of red betel leaves were obtained from Bogor Agricultural University's biopharmaceutical. The leaves were sorted and dehydrated in a 50 °C oven. The leaves were then mashed and strained through 60-mesh sieves. The extraction of red betel leaves uses the maceration method as described by Safithri et al. with modifications (Safithri et al., 2015). The 300 g simplicial was dispersed in 70% ethanol at room temperature with a speed of 130 rpm for 24 h. At 50 °C, the crude extract was filtered and concentrated using a rotary evaporator. The fractionation of ethanol extract was performed according to the method described by Firdausi et al. (Firdausi et al, 2015). Based on the polarity stage, fractionation was performed using non-polar n-hexane, semi-polar ethyl acetate, and polar distilled water in a 1:1 ratio to each solvent. Approximately 1 g of ethanol extract was diluted with 900 mL of distilled water and poured into a separate funnel. Then 900 mL of n-hexane is added and homogenized by horizontally rotating the funnel for 5 min. The mixed solution was then incubated to make two layers of n-hexane and water, which were then separated. In the ethyl acetate fraction, 900 mL of ethyl acetate was added to the water fraction and homogenized for 5 min. The mixture was incubated until two distinct layers appeared and separated. The n-hexane, ethyl acetate, and water fraction were evaporated using a rotary evaporator.

2.3. Tyrosinase inhibition

The tyrosinase inhibition assay was conducted following the methods described by Batubara et al. (Batubara et al., 2010) and GD et al. (Liyanaarachchi et al., 2018) with modifications. The reaction mixture consisted of 50 mM sodium phosphate buffer (pH 6.5), 333 U/mL of mushroom tyrosinase (EC 1.14.18.1), and 2 mM L-tyrosine. The red betel ethanol extract, ethyl acetate fraction, n-hexane fraction, and water fraction were prepared at 625, 1250, 2500, 5000, and 10000 ppm. Kojic acid was used as a positive control. In triplicate, 70 μL of each sample's dilution was combined with 30 μL of tyrosinase in a 96-well plate. After incubating at room temperature for 5 min, 110 μL of L-tyrosine was added to each well. The mixture was further incubated at

room temperature for 30 min. The optical densities of the wells were measured using a multi-well plate reader at 475 nm. The tyrosinase inhibitory effect of the extract and fractions was determined as the 50% inhibitory concentration (IC_{50}).

2.4. UHPLC-q-orbitrap HRMS

The active component of red betel is analyzed utilizing the UHPLC Vanquish system in conjunction with mass spectrometry Q Exactive Plus Orbitrap HRMS. Accucore C18, 100 × 2.11 mm, 1.5 m particle size (Thermo ScientifcTM Waltham, MA, USA), 30 °C. As mobile phases, 0.1 formic acid in water (A) and 0.1% in acetonitrile were used. The eluent gradient environment consisted of 5% B for one minute, 5–95% B for one to fifteen minutes, 95% B for 25 to 28 min, and 5% B for 28 to 30 min. The MS1 settings were *m/z* 100–1000 (mass range), 70.000 (resolution), and $1x10^{-6}$ (target AGC). MS2 was configured with a 17,500 resolution and an AGC 1x 10–5 (N)CE target of 18,35,53. The analysis was conducted in positive and negative ionization modes, utilizing sheath flow gas, gas aux 3, spray voltage 3.8 kV, compiler temperature 320 °C, and level RF lens S50.

2.5. Molecular docking

The three-dimensional structures of the data-set ligands were derived from PubChem and drawn with Discovery Studio (Biovia, 2017). All polar hydrogen was added, non-polar hydrogen was merged, and Gasteiger charges were added using Auto Dock 4.2 (Huey et al., 2012). The 3D structures of mushroom tyrosinase were obtained from RCSB Protein Data Bank (PDB ID: 2Y9X). The protein was separated from its native ligand (tropolone), added polar hydrogen, merged non-polar hydrogen, and added Kollman charge (Wang et al., 2006). The molecular docking analysis uses Autodock in Pyrx (Dallakyan and Olson, 2015). The parameters for the protein grid box were × = -10.043, y = -28.706, and z = -43.443, and the grid box volume was 15 Å x 15 Å x 15 Å. Co-crystallized ligand, and the docked native were superimposed to validate the docking process.

2.6. Drug likeness and ADMET prediction

In this study, we evaluated the absorption, distribution, metabolism, excretion, and toxicity (ADMET) properties, along with the physicochemical parameters related to drug-likeness, such as Lipinski's 'rule of five,' skin permeability (Log Kp) and skin sensitization, for the selected hit compounds. The ADMET properties and drug-likeness descriptors were assessed using well-established computational tools, including the swissADME (https://www.swissadme.ch/) and pkCSM web servers (https://biosig.unimelb.edu.au/pkcsm) (Daina et al., 2017; Pires et al., 2015). The data input was in SMILES format, retrieved from the PubChem database and using Discovery Studio (Biovia, 2017).

2.7. Molecular dynamic

Simulations of protein–ligand molecular dynamics were conducted using GROMACS version 2021.5. (Abraham et al., 2015). Tropolone as the native ligand, kojic acid as the positive control, and the selected red betel ligands were input into the PDB format. The ligand topology was built using the Swissparam webserver (Zoete et al., 2011). Meanwhile, the protein topology was generated using Charmm36 in the Gromacspdb2gmx package (da Silva et al., 2022). The complex was immersed in the cubic box (x, y, and z) with a minimum distance of 1 nm between the protein surface and the box walls, followed by salvation in a simple point-charge water molecule. The net charge of the system was neutralized by adding $Na^{+}Cl^{-}$ ions. The entire system is then subjected to energy minimization using the steepest decent algorithm with a 1000 kJ/mol/nm tolerance. Two constrained phases were equilibrated with the solvent and ion. The system is next passed through the NVT (isothermal-isochoric) ensemble at 300 K and the NPT (isothermal-isobaric) ensemble at 1 bar pressure. The Particle Mesh Ewald Method was utilized to compute the long-range electrostatic interaction (Essmann et al., 1995). LINCS (Linear Constraint Solver) was employed to restrict the bond length (Hess et al., 1997). The MD simulations were performed at constant temperature and pressure for 100 ns.

2.8. Statistical analysis

The statistical analyses were conducted using SPSS software. One-way analysis of variance (ANOVA) was employed, followed by Tukey's honestly significant difference (HSD) posthoc test. Significant differences were considered at P values less than 0.05.

3. Result

3.1. Extraction and fractionations of red betel leaves

The yield of ethanol extract, n-hexane, ethyl acetate, and water fraction was 6.40%, 0.67%, 1.74%, and 2.16%, respectively. It was observed that the ethanol extract has the most significant percentage yield. In contrast, the n-hexane fraction has yield the least among the extract and other fractions of red betel leaves.

3.2. Evaluation of tyrosinase inhibition

The extract and fractions of red betel leaves were tested and compared to the positive control kojic acid to determine their tyrosinase inhibitory capability. The IC_{50} is also observed to analyze the inhibitory profile by serial dilution of red betel extract, fractions, and kojic acid at concentrations ranging from 625 ppm to 10000 ppm.

The significant difference in IC_{50} values between the ethanol extract, ethyl acetate fraction, and water fraction when compared to the n-hexane fraction highlights the varying degrees of tyrosinase inhibition exhibited by these fractions. The IC_{50} of the n-hexane fraction significantly differred from the other tested ethanol and other fraction with the value of 217874 ± 30069. Notably, the water fraction demonstrated robust inhibition of tyrosinase activity with an IC_{50} value of 6344 ± 55. Although the inhibitory effect of the water fraction was not as potent as that of the positive control kojic acid (IC_{50} 15.83 ppm), its notable inhibitory potential warrants further investigation (see Table 1).

3.3. UHPLC-q-orbitrap HRMS analysis

The *in vitro* analysis showed that the red betel leaves' water fraction exhibited the highest tyrosinase inhibitory activity compared to the other extract fractions. UHPLC-Q-Orbitrap HRMS analysis was performed on the phenolic compounds to investigate the active constituents further. As shown in Table 2, twenty active compounds were identified and characterized.

3.4. Molecular docking

Molecular docking is a reliable tool in biological research for

Table 1
IC_{50} of red betel extract and fractions against tyrosinase.

Samples	IC_{50} (ppm)
Ethanol extract	7780 ± 1260^{bc}
Ethyl acetate fraction	8026 ± 212^{c}
Water fraction	6344 ± 55^{b}
Kojic acid	15.83 ± 1.96^{a}

The results were presented as the means of triplicate assays with standard deviation (SD). Superscript letters (a, b, c) indicate significant differences at a *p* value less than 0.05.

Table 2
Compounds identified by UHPLC-Q-Orbitrap HRMS analysis of red betel leaves water fraction.

Retention Time (min)	Compounds	*m/z*	Molecular Formula
4.928	Trans-3-Indoleacrylic acid	187.0629	$C_{11}H_9NO_2$
5.271	N-*trans*-feruloyl tyramine	313.1307	$C_{18}H_{19}NO_4$
5.5	Trichostachine	271.1203	$C_{16}H_{17}NO_3$
6.685	(-)-*trans*-carveol	152.1199	$C_{10}H_{16}O$
6.85	(+)-Blumenol A	224.1407	$C_{13}H_{20}O_3$
6.876	Piperine	285.1358	$C_{17}H_{19}NO_3$
6.957	Piperamide-C7:2 (2E,6E)	299.1516	$C_{18}H_{21}NO_3$
7.357	N-Methyllaurotetanine	341.1619	$C_{20}H_{23}NO_4$
8.208	Kaempferitrin	578.1622	$C_{27}H_{30}O_{14}$
8.34	Rutin	610.1531	$C_{27}H_{30}O_{16}$
9.322	(-)-Dihydroclusin	404.1819	$C_{22}H_{28}O_7$
9.353	Byzantionoside B	372.2142	$C_{19}H_{32}O_7$
9.905	Kadsurin B	374.1722	$C_{21}H_{26}O_6$
10.035	2,4,5-Trimethoxystyrene	194.0937	$C_{11}H_{14}O_3$
12.184	Futoquinol	354.1451	$C_{21}H_{22}O_5$
12.189	(+)-Yangambin	446.1929	$C_{24}H_{30}O_8$
14.143	β-asarone	208.109	$C_{12}H_{16}O_3$
16.882	α-asarone	208.1092	$C_{12}H_{16}O_3$
16.884	Methyl 3,4,5 - trimethoxycinnamate	252.099	$C_{13}H_{16}O_5$
17.935	Piperkadsin B	430.1976	$C_{24}H_{30}O_7$

identifying the favorable binding interactions between a ligand (small molecule) and a receptor (protein) to predict their potential interactions (De Ruyck et al., 2016). In this study, our objective was to identify a molecule from the water fraction that interacts with the active site of tyrosinase. To validate the docking protocol, we performed molecular docking calculations using the crystal structure of mushroom tyrosinase bound to tropolone (PDB ID: 2Y9X). Tropolone, the co-crystallized ligand, was re-docked into the tyrosinase protein structure resulting in a superimposition of 2.09 Å over the native conformation (Fig. 1).

In molecular docking analysis, the best ligand is determined based on the binding free energy value. Binding free energy, also known as binding affinity (ΔG), represents the energy released during the formation of bonds or interactions between the protein and ligand. It directly influences the stability of the receptor-ligand complex, with a negative value indicating a more stable complex (Vita et al., 2021).

Molecular docking utilizes a scoring function to generate a score for each pose, providing a fast and approximate binding affinity estimation (Pantsar and Poso, 2018). The docking analysis results are represented as docking scores in kcal/mol, indicating the energy released during protein–ligand binding. It has been established that the more negative the score, the stronger the binding affinity (Trott and Olson, 2010). Therefore, ligands with the highest affinity (more negative docking scores) can be selected as potential leads for further studies.

In our study, the molecular docking results revealed three compounds with docking scores below −6.5, indicating vigorous binding activity with tyrosinase (Table 3). Among them, piperine, piperamide-C7:2 (2E,6E), and trichostachine displayed significantly lower docking scores of −7.04, −6.87, and −6.79 kcal/mol, respectively, suggesting stronger binding affinity compared to the native ligand tropolone and the control kojic acid, with docking scores of −4.56 and −4.30 kcal/mol, respectively. These three red betel water fraction hit compounds show potential as tyrosinase inhibitors.

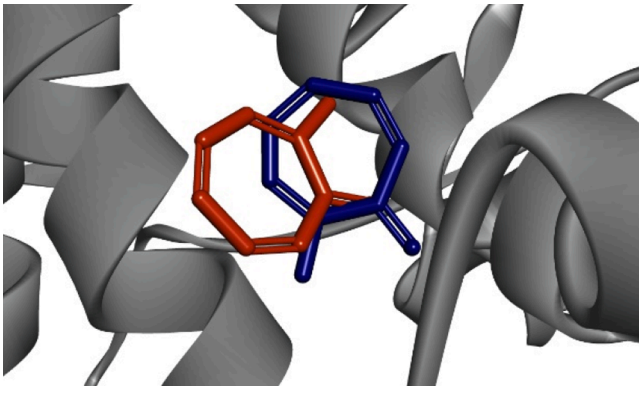

Fig. 1. Superimposed of co-crystalized ligand tropolone (orange) and docked ligand (blue).

The docking analysis further indicated that tropolone, kojic acid, piperine, piperamide-C7:2 (2E,6E), and trichostachine were observed in the docked poses, suggesting their binding to the catalytic pocket of tyrosinase (Fig. 2). Tropolone displayed significant interactions with active residues, forming hydrogen bonds with Met280 and Ser282, and hydrophobic bonds with Val283 and Ala286. It also formed a pi-cation interaction with His263. Van der Waals interactions were observed with residues including His61, His85, His259, Asn260, Phe264, His279, Gly281, and Phe292 (Fig. 2B). For the binding modes of kojic acid and

Table 3
Predicted docking score and detailed interaction of tropolone, kojic acid, and water fraction compounds were attached to tyrosinase (2Y9X).

Compounds	Binding Energy (Kcal/mol)	H-Bond	Hydrophobic bond
Tropolone (Native ligand)	−4.56	Met280, Ser282	Val283, Ala286
Kojic acid	−4.30	His259, Met280, His296	Val283, Ala286
Trans-3-Indoleacrylic acid	−5.14	His85, His94, His296	Val283, Ala286
N-*trans*-feruloyltyramine	−6.13	His61, Asn81, His85, His244, Asn260	Val283, Ala286
Trichostachine	−6.79	His61	Val283, Ala286, Pro277
(-)-*trans*-carveol	−5.34	Val283	Phe264
(+)-Blumenol A	−5.54	Val283, Gly281	His263, Phe264
Piperine	−7.04	His61	Pro277, Val283, Ala286
Piperamide-C7:2 (2E,6E)	−6.87	Asn81, His85	His263, His61, His244, Val283, Ala286
N-methyllaurotetanine	−5.98	–	Val283, Phe264, His61, His263, Pro277, Ala286
Kaempferitrin	−3.04	Arg268, Val283, Glu322	Phe264, Val248
Rutin	−3.66	Ser282, Glu322	Val283, His85, His263
(-)-Dihydroclusin	−5.14	Asn260, His263	Val283, Ala286
Byzantionoside B	−5.84	Val282, Val283	Val283, Val248, Pro284
Kadsurin B	−6.00	–	Phe264, Val283, Ala286
2,4,5-trimethoxystyrene	−4.92	–	Phe264, Val283, His61, His94, Phe292, His296
Futoquinol	−6.36	Asn81, His85	His61, His263, Val283, Ala286
(+)-Yangambin	−4.18	Asn81, His85, Arg268	Val283, Val248, Pro284
β-asarone	−4.99	–	His263, Phe264, Val283, His61, Phe90, His94, His244, Phe292, His296
α-asarone	−4.99	His244	His263, Val283, His61, His94, Val248, Phe264, His259, Phe292, His296
Methyl 3,4,5 – trimethoxy cinnamate	−5.02	His259, His263, His296	His85, Val283, His244
Piperkadsin B	−4.59	–	His263, His283, Val248

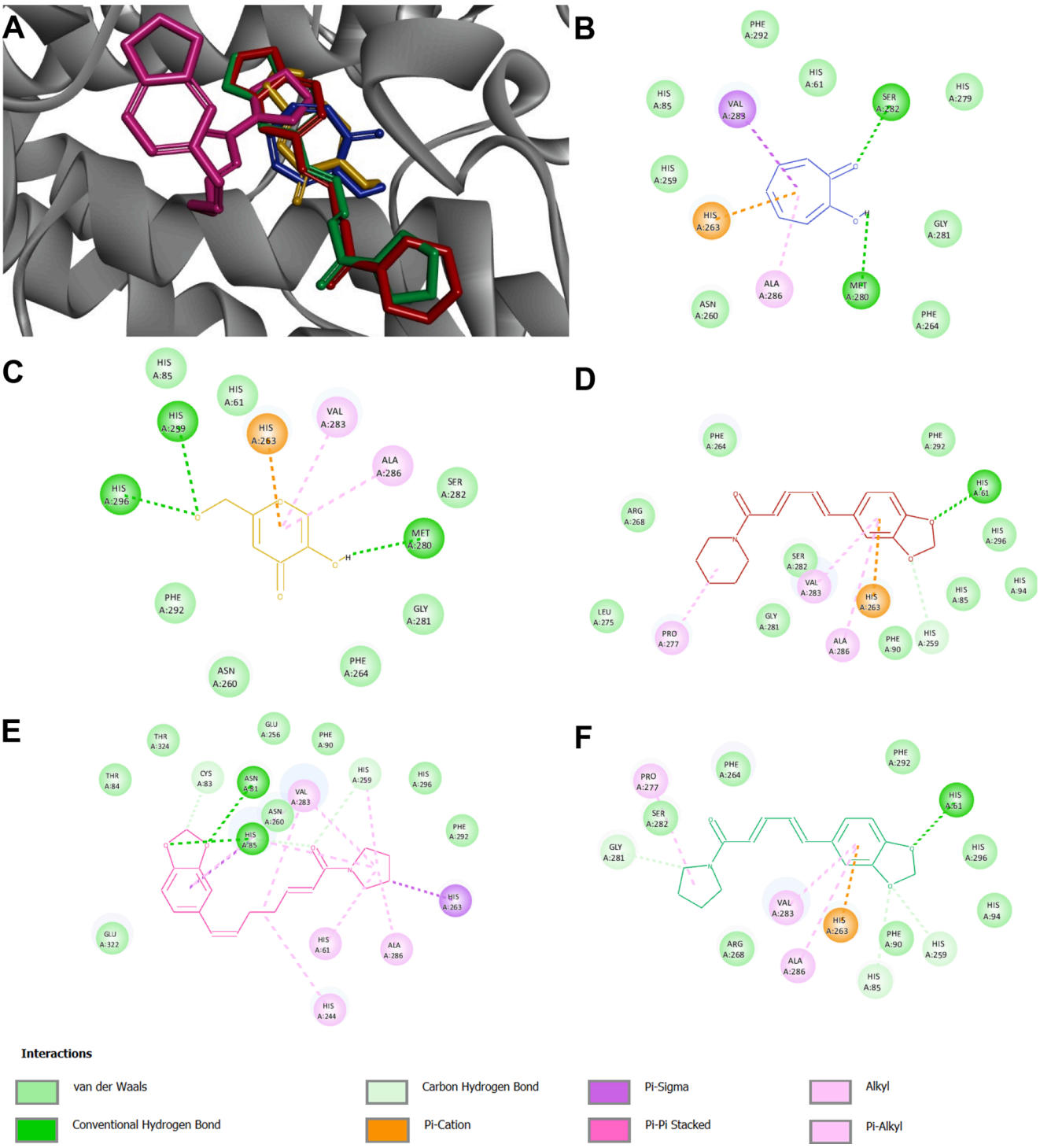

Fig. 2. (A) Superposition of tropolone (blue), kojic acid (orange), piperine (red), piperamide-C7:2 (2E,6E) (pink), and trichostachine (green) inside the binding cavity of mushroom tyrosinase. Amino acid interaction of tyrosinase with (B) tropolone, (C) kojic acid, (D) piperine, (E) piperamide-C7:2 (2E,6E), and (F) trichostachine.

tyrosinase, (Fig. 2C), amino acid residues His259, Met280, and His296 formed hydrogen bonds, estabilishing a hydrophobic bond with Val283 and Val286. Van der Waals interactions with His61, His85, Asn260, Phe264, Gly281, Ser282, and Ser292.

Piperine exhibited hydrogen contacts with Asn81 and His85 and hydrophobic interactions with His61, His244, His263, and Val283. Similarly, piperamide-C7:2 (2E,6E) also showed hydrogen contacts with Asn81 and His85, and exhibited hydrophobic interactions with His61, His244, His263, and Val283. Furthermore, trichostachine formed a hydrogen bond with His61 and engaged in hydrophobic interactions with Ala286, Val283, and Pro277. The selected hit compounds piperine, piperamide-C7:2 (2E,6E), trichostachine, tropolone, and kojic acid were further investigated.

3.5. *Drug likeness and in silico ADMET properties*

The evaluation of the potential red betel leaves compounds, namely piperine, piperamide-C7:2 (2E,6E), and trichostachine, for their ADMET

physicochemical properties using SwissADME and pKCSm revealed promising findings (Table 4). All three compounds complied with the Lipinski rule, indicating their potential as drug-like molecules. This rule considers molecular weight, Log P, H-bond donors, H-bond acceptors, and molar refractivity (Lipinski et al., 1997).

3.6. Molecular dynamic

The mere observation of a ligand–protein interaction in docking does not guarantee the stability of the ligand within the protein's binding pocket. Therefore, further investigation and validation of the results are necessary. Molecular dynamics (MD) simulation is valuable for addressing these limitations. It enables predicting atomic movements in a molecular system based on physics-based intermolecular interactions. By considering solvent effects, sampling different conformations, and assessing receptor clustering, MD simulations can account for the conformational changes of the protein and provide a more comprehensive evaluation of ligand stability. MD simulations create an environment that better evaluates a drug candidate's stability within an enzyme's binding pocket by simulating the behavior of a docked ligand–protein complex. The resulting trajectories generated from the simulation provide valuable insights into parameters crucial for strong and stable interaction. Key metrics analyzed from these trajectories include root mean square deviation (RMSD), root mean square fluctuation (RMSF), radius of gyration (Rg), and solvent-accessible surface area (SASA) (Tripathi et al., 2022; Syaifie et al., 2022).

In our current study, the RMSD (Fig. 2A) for the complex tyrosinase-tropolone complex was consistent for the first 57 ns, fluctuated slightly with an average RMSD of 0.4 nm for the next 67 ns, and stayed unchanged until the end of the MD simulation. In the tyrosinase–kojic acid interaction, this compound was stable up to 56 ns and fluctuated significantly up to 62 ns. However, it stays constant with an average RMSD of 0.3 nm until 100 ns. The protein-piperine appeared to fluctuate slightly from the starting point to the end of the simulation, with an average RMSD value of 0.5 nm. The tyrosinase-piperamide-C7:2 (2E,6E) RMSD value increased to 13 ns but remained relatively stable until 100 ns MD simulation, at an average of 0.9 nm. At 32 ns, the interaction between tyrosinase and trichostachine produced a substantial deviation up to 2.1 nm. All through the the simulation, the RMSD value averaged 1.4 nm.

The simulated protein and protein–ligand complex exhibit notable conformational fluctuations in a particular tyrosinase residue. The residue Leu75 was observed to be flexible in both the apoprotein and the whole protein–ligand complex. The interaction involving protein and tropolone at Val248 and 0.57 nm displayed most tremendous significant variation. The tyrosinase-trichostachine also resulted in a rise in the RMSF value of the Gly392 residue at 0.70 nm.

Fig. 5 illustrates the change in Rg values for tyrosinase apoprotein and the ligand. The average Rg values for tyrosinase, tyrosinase-tropolone, tyrosinase-kojic acid, tyrosinase-piperine, tyrosinase-piperamide-C7:2 (2E,6E), and tyrosinase-trichostachine were 2.08, 2.08, 2.07, 2.07, and 2.08 nm, respectively.

Fig. 6 demonstrates the SASA analysis of the apoprotein and the protein–ligand complex. The average SASA of the apoprotein was 179 nm. The protein-tropolone complex displayed a greater average SASA value of 181 nm compared to the protein-kojic acid complex, which had a lower average SASA value of 177 nm. The SASA values of tyrosinase-piperine and tyrosinase-trichostachine were close to that of the native tyrosinase, with an average of 197 nm. However, the tyrosinase-piperamide-C7:2 (2E,6E) complex exhibited the lowest SASA value among the protein and protein–ligand complexes, with an average SASA value of 175 nm. This significant reduction in SASA indicates a tightly folded protein conformation, resulting in decreased solvent accessibility.

Table 4
Drug-likeness and ADMET prediction of three selected red betel leaves compounds.

Properties	Piperine	Piperamide-C7:2 (2E,6E)	Trichostachine
MW (g/mol)[a]	285.34	299.36	271.31
H-bond acceptors[b]	3	3	3
H-bond donors[c]	0	0	0
MLogP[d]	2.39	2.62	2.14
Molar Refractifity[e]	85.48	90.28	80.67
RO5[f]	0	0	0
log Kp (cm/s)[g]	−5.58	−5.50	−5.75
Skin Sensitization[h]	NO	NO	NO

[a] Molecular Weight (acceptable range 130–500 gm/mol).
[b] Acceptable H-bonds (acceptable range 0–10).
[c] Donatable H-bonds (acceptable range 0–5).
[d] MLOGP (acceptable range 0–5).
[e] Molar Refractivity.
[f] Rule of Five.
[g] Skin permeant (Acceptable range (−8) - (−1)).
[h] Predicted skin sensitization.

4. Discussion

4.1. Extraction and fractionations of red betel leaves

The yield of red betel leaves ethanol extract obtained in this study was 6.40% lower than the yield of red betel leaves ethanol extract from the same place, which is 15.55%. The yield of red betel leaves n-hexane, ethyl acetate, and water fractions were 0.67%, 1.74%, and 2.16%, respectively. This result is lower than the yield of red betel leaves fractions from the same place and the same solvent, which is 1.81%, 3.52%, and 9.49%, respectively (Zaelani, n.d.). The difference between extraction and fractions yield could be influenced by the extraction time extraction methods, part of the sample used, solvent types, ratios between the number of samples and solvents, extraction temperatures, and particle sizes of the sample (Fan et al., 2015; Li et al., 2021; Moorthy et al., 2015).

An excellent yield of pectin extraction from *Punica granatum* was achieved using a solid–liquid ratio of 1:17.52 g/mL at a temperature of 61.90 °C, with a total extraction time of 28.31 min (Moorthy et al., 2015). In the case of *Hibiscus cannabinus* L. leaves, using water as a solvent resulted in a significantly increased extract yield of 28% compared to methanol, ethanol, and acetone (Sim et al., 2019). Moreover, a notable difference was observed in the extraction yield of polysaccharides from mulberry fruits (*Morus alba* L.) when a superfine grinding process was applied as a pretreatment. It was found that smaller particles of mulberry powder led to improved extraction yields. Specifically, polysaccharides extracted from the pre-treated mulberry powder using high-speed shear homogenization-assisted hot water extraction exhibited superior antioxidant activity compared to those obtained directly from mulberry fruits (Li et al., 2021).

4.2. Evaluation of tyrosinase inhibition

The tyrosinase inhibition analysis results demonstrate the varying degrees of tyrosinase inhibition exhibited by the different fractions of red betel leaves. Despite not showing a significant difference between the ethanol extract and ethyl acetate fraction, the water fraction demonstrated significant differences from the n-hexane fraction, which exhibited an IC_{50} value of 217874 ± 30069. In particular, the water fraction of red betel leaves displayed solid inhibitory against tyrosinase, with an IC_{50} value of 6344 ± 55. Although its inhibitory effect was less potent than kojic acid (IC_{50}: 15.83 ppm), the water fraction still exhibited a lower IC_{50} value than the ethanol extract and other red betel fractions.

Aziz, (2022) reported that the ethyl acetate extract of wungu leaves at a concentration of 10,000 ppm exhibited inhibited 37.94 ± 16.50% of tyrosinase activity. In comparison, the methanol and water extract of

wungu leaves at the same concentration showed inhibitions of 19.72 ± 10.80% and 16.82 ± 3.05%, respectively. These results suggest that both the ethanol extract and water fraction, as well as the ethyl acetate fraction of red betel leaves, possess more robust tyrosinase inhibitory activity than wungu leaves extracts (Aziz, 2022).

Given the superior inhibition activity of the water fraction among the ethanol extract and other fractions, it was selected for further characterization of its constituent compounds. Additionally, an in silico study was conducted to predict the role of these compounds in tyrosinase inhibition.

4.3. UHPLC-q-orbitrap HRMS analysis

Some of the compounds found in red betel leaves, especially in the water fraction in the present study, were also present in other medicinal plants. The organic acid *trans*-3-indoleacrylic acid is also found in coffee leaf extract (Mei and Chen, 2023). N-*trans*-feruloyl tyramine was found in the root extract *of Smilax aristolochiifolia*, *Lycium barbarum* fruit extract, *Bassia indica,* and *Agathophora alopecuroides* extract, and Cherimoya (*Annona cherimola* Mill.) (Amaro et al., 2014; Galarce-Bustos et al., 2019; Khan et al., 2021; Othman et al., 2022). It exhibited significant activity as an α-glucosidase inhibitor and demonstrated anti-aggregation effects on amyloid-beta fibrils, indicating its potential for Alzheimer's disease therapy.

The compound piperine is an alkaloidal chemical compound found in the *Piper longum*, *Piper nigrum*, belonging to the *Piperaceae* family (Tiwari et al., 2020). It was found in several parts of the plant, including fruit, spike, roots, stem, and leaves (Haq et al., 2021). It exhibits promising antimalarial effects against both chloroquine-sensitive and chloroquine-resistant strains of Plasmodium falciparum, shows cytotoxicity against human brain cancer cells, and holds potential as an anti-aging compound due to its photoprotective and anti-inflammatory properties (Jaisin et al., 2020; Sedeky et al., 2018; Thiengsusuk et al., 2018). (Tiwari et al., 2020). It was found in several parts of the plant including fruit, spike, roots, stem as well as leaves (Haq et al., 2021). It exhibits promising antimalarial effects against both chloroquine-sensitive and chloroquine-resistant strains of *Plasmodium falciparum*, shows cytotoxicity against human brain cancer cells, and holds potential as an anti-aging compound due to its photoprotective and anti-inflammatory properties (Jaisin et al., 2020; Sedeky et al., 2018; Thiengsusuk et al., 2018).

The compound Piperamide-C7:2 (2E,6E), commonly found in food, dietary supplements, and herbal products, was predicted as a potential CYP3A4 inhibitor using a deep-learning model [10]. Additionally, trichostachine, a compound found in *Piper nigrum*, exhibits antibacterial activity by inhibiting quorum sensing (Ngo et al., 2018; Vázquez-Martínez et al., 2020). Meanwhile, the neolignans compounds such as futoquinol and piperkadsin B were mainly found in *Piper kadsura* that have been tested for potent anti-inflammatory activity (Lin et al., 2006).

4.4. Molecular docking

The docking analysis was performed for the twenty compounds with the Autodock in PyRx software with the tyrosinase retrieved from the Protein Data Bank (PDB: 2Y9X). The docking protocol was validated by superimposing the co-crystallized ligand tropolone with the docked ligand. The obtained superimposition value was 2.09 Å (Fig. 1), indicating the validity of the used docking protocol (Ramírez and Caballero, 2018). This suggests that the docking procedure effectively captures the binding interactions between tyrosinase and the tested compounds.

The ideal compounds could fit well to the binding site, which showed by the lowest docking score and favorable interactions. As shown on Table 2 and Fig. 2, piperine, piperine, piperamide-C7:2 (2E,6E), and trichostachine depicted favorable docking scores compared to tropolone and kojic acid, suggesting the potential for better inhibitory activity.

In tyrosinase, the HIS residue is well-known for directly interacting with Cu in the catalytic site (Ismaya et al., 2011). In our study, piperine formed a hydrogen bond with His61 and established four hydrophobic bonds with His263, Val283, Ala286, and Pro277. This finding is consistent with a previous study by Yu et al. (2019) which reported hydrophobic bonds between quercetin, another compound targeting tyrosinase, and VAL283 and ALA286 (Yu et al., 2019). Meanwhile, the piperamide-C7:2 (2E,6E) is engaged in hydrophobic contacts with His61, His244, His263, and Val283. Furthermore, trichostachine formed a hydrogen bond with HIS61 and engaged in hydrophobic interactions with Ala286, Val283, and Pro277.

4.5. Drug likeness and in silico ADMET properties

The results obtained from evaluating ADMET physicochemical properties provide valuable insights into the potential of piperine, piperamide-C7:2 (2E,6E), and trichostachine as anti-tyrosinase drugs. Compliance with Lipinski's rule of five suggests that these compounds possess favorable pharmacokinetic properties, making them more likely to be membrane-permeable and have high bioavailability after oral administration. It is particularly relevant for drug development, as compounds that meet these criteria are often associated with improved chances of success.

Moreover, the good skin permeability demonstrated by the compounds indicates their potential to penetrate the skin barrier effectively. This characteristic can be advantageous for topical formulations or transdermal drug delivery, where efficient skin permeability is crucial for achieving therapeutic effects.

The absence of skin-sensitizing properties further enhances the appeal of these compounds. Skin sensitization can lead to adverse reactions and limit the usability of a drug candidate. By demonstrating a lack of sensitizing potential, piperine, piperamide-C7:2 (2E,6E), and trichostachine promise safety and reduced risk of adverse skin reactions.

4.6. Molecular dynamic

Molecular dynamics (MD) simulation aims to recreate the actual behavior of molecules in their surroundings, taking their pliability and mobility into account (Durrant and McCammon, 2011). These simulations provide information on particle movements as a function of time (Karplus and McCammon, 2002).

In this study, 100 ns of MD simulations were conducted to explore the stability and conformational changes of tyrosinase and its interactions with tropolone, kojic acid, piperine, piperamide-C7:2 (2E,6E), and trichostachine. The parameters investigated were RMSD, RMSF, Rg, and SASA.

RMSD (root mean square deviation) is a valuable measure for assessing the equilibrium and stability of MD trajectories (Martínez, 2015). As depicted in Fig. 3, the RMSD analysis revealed the overall stability of tyrosinase and its complexes with the inhibitors over the 100 ns simulation. The protein-tropolone complex and the tyrosinase-kojic acid interaction exhibited relatively stable RMSD values, suggesting intense binding and minimal structural changes. In contrast, the protein-piperine complex showed slight fluctuations, indicating a more dynamic interaction.

The RMSF (root mean square fluctuation) analysis is used to characterize the protein's flexibility and identify dynamic residues (Abdalla et al., 2022). Interestingly, in every MD simulation, there was no significant increase in the concentration of amino acid residues in the HIS residues 61, 85, 94, 259, 263, and 296, which are the sites that interact directly with Cu (Ismaya et al., 2011). It implies that the binding of the inhibitors did not significantly affect the dynamic behavior of these critical residues (see Fig. 4).

The compactness of tyrosinase and its complexes with the inhibitors was determined by comparing their radius of gyration (Rg) (Sneha and Doss, 2016). The Rg analysis demonstrated that the apoprotein and the simulated protein–ligand complexes maintained high compactness.

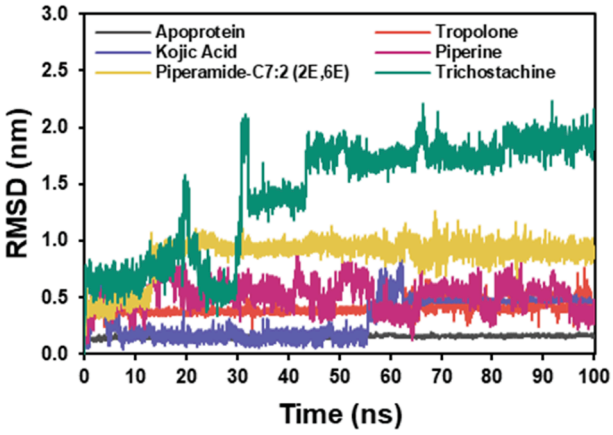

Fig. 3. RMSD plot of the docked complex structure of tyrosinase with tropolone (blue), kojic acid (orange), piperine (red), piperamide-C7:2 (2E,6E) (pink), and trichostachine (green).

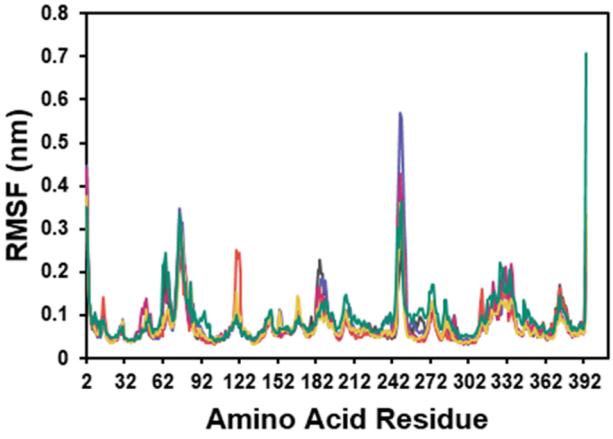

Fig. 4. RMSF plot of the docked complex structure of tyrosinase with tropolone (blue), kojic acid (orange), piperine (red), piperamide-C7:2 (2E,6E) (pink), and trichostachine (green).

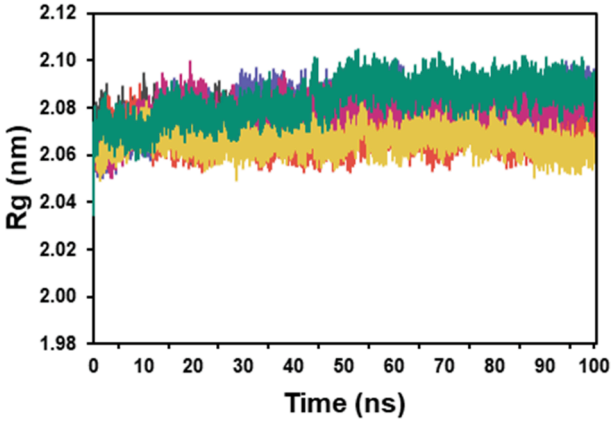

Fig. 5. Rg plot of the docked complex structure of tyrosinase with tropolone (blue), kojic acid (orange), piperine (red), piperamide-C7:2 (2E,6E) (pink), and trichostachine (green).

There was no significant difference in the Rg values, indicating that the binding of the inhibitors did not cause substantial changes in the overall structure and compactness of tyrosinase.

SASA (solvent-accessible surface area) analysis is assessed to study protein accessibility and the interaction with solvent molecules (Liu et al., 2019). The SASA analysis provided insights into the solvent accessibility of tyrosinase and its complexes. The protein-tropolone complex showed a higher SASA value, indicating increased exposure to the solvent compared to the protein-kojic acid complex. The SASA values of tyrosinase-piperine and tyrosinase-trichostachine were similar to that of the neat tyrosinase, suggesting that these inhibitors did not significantly affect solvent accessibility. However, the tyrosinase-piperamide-C7:2 (2E,6E) complex exhibited a lower SASA value, indicating a tighter folding and reduced solvent accessibility.

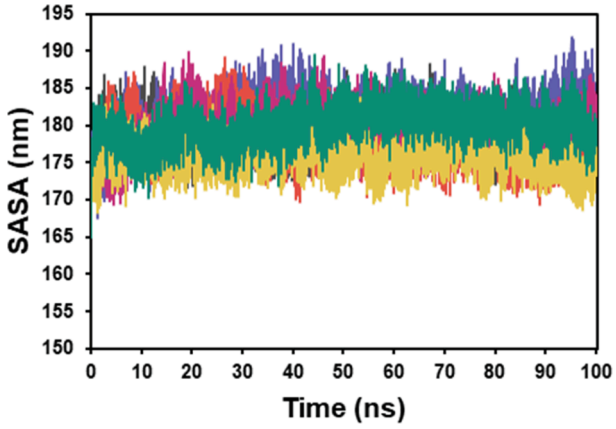

Fig. 6. SASA plot of the docked complex structure of tyrosinase with tropolone (blue), kojic acid (orange), piperine (red), piperamide-C7:2 (2E,6E) (pink), and trichostachine (green).

5. Conclusion

In the present study, extraction of the bioactive compounds of red betel leaves has been performed with 70% ethanol. The ethanol extract undergoes fractionation with different solvents. All the extracts and fractions were evaluated for inhibitory activity against mushroom tyrosinase. Among the extract and all the fractions, the water fraction showed promising activity in tyrosinase inhibition. This fraction undergoes UHPLC to investigate the active compounds. Based on molecular docking analysis, the compound piperine, piperamide-C7:2 (2E,6E), and trichostachine were the most potent inhibitors among all the water fraction compounds. The molecular dynamics analysis investigation showed that piperine was the most stable compound among the three compounds tested.

Author contribution

M.S.*, D.A. contributed to conceptualization, resources, data curation, and funding acquisition. A.G.A contributed to writing - original draft, methodology, formal analysis, and data curation. P.H.S** contributed to conceptualization, methodology, data curation, investigation, and writing-review and editing. N.M.N.K. contributed to methodology and formal analysis. E.M.*** provided conceptualization, supervision, writing- review and editing. D.N/M.M.F/W.D.N. contributed to software, data curation, and formal analysis. D.A.S./L.T.M./M.H./E.S. participated in methodology and formal analysis. R.A.P.I. assisted with data curation and writing-original draft. N.T.R. oversaw the project with supervision, and resources.

Declaration of competing interest

The authors declare that they have no known competing financial interests or personal relationships that could have appeared to influence the work reported in this paper.

Acknowledgment

This work was funded by the Indonesia Directorate General of Higher Education, Research, and Technology [3881 /IT3.L1/PT.01.03/P/B/2022]. The Authors thanks to Department of Biochemistry, Faculty of Mathematics and Natural Science, Bogor Agricultural University and Nano Center Indonesia, for providing the facilities needed for this research.

Appendix A. Supplementary data

Supplementary data to this article can be found online at https://doi.org/10.1016/j.jksus.2023.102933.

References

Abdalla, M., Eltayb, W.A., El-Arabey, A.A., Singh, K., Jiang, X., 2022. Molecular dynamic study of SARS-CoV-2 with various S protein mutations and their effect on thermodynamic properties. Comput. Biol. Med. 141, 105025.

Abraham, M.J., Murtola, T., Schulz, R., Páll, S., Smith, J.C., Hess, B., Lindahl, E., 2015. GROMACS: High performance molecular simulations through multi-level parallelism from laptops to supercomputers. SoftwareX 1, 19–25.

Amaro, C.A.B., González-Cortazar, M., Herrera-Ruiz, M., Román-Ramos, R., Aguilar-Santamaría, L., Tortoriello, J., Jiménez-Ferrer, E., 2014. Hypoglycemic and hypotensive activity of a root extract of Smilax aristolochiifolia, standardized on N-trans-feruloyl-tyramine. Molecules 19, 11366–11384.

Ando, H., Matsui, M.S., Ichihashi, M., 2010. Quasi-drugs developed in Japan for the prevention or treatment of hyperpigmentary disorders. Int. J. Mol. Sci. 11, 2566–2575.

Aziz, A. Dimas, M, A. Safithri, 2022. Penambatan Molekuler dan Studi In Vitro Senyawa Bioaktif Daun Wungu (Graptophyllum pictum (L) Griff) sebagai Inhibitor Tirosinase. Indonesian Journal of Pharmaceutical Science and Technology 9, 96–107.

Ball Arefiev, K.L., Hantash, B.M., 2012. Advances in the treatment of melasma: a review of the recent literature. Dermatologic Surg. 38, 971–984.

Batubara, I., Darusman, L.K., Mitsunaga, T., Rahminiwati, M., Djauhari, E., 2010. Potency of Indonesian medicinal plants as tyrosinase inhibitor and antioxidant agent. J. Biol. Sci. 10, 138–144.

Biovia, D.S., 2017. Discovery studio modeling environment.

Chandra, M., Levitt, J., Pensabene, C.A., 2012. Hydroquinone therapy for post-inflammatory hyperpigmentation secondary to acne: not just prescribable by dermatologists. Acta Derm. Venereol. 92.

Costa, T.G., Feldhaus, M.J., Vilhena, F.S., Heller, M., Micke, G.A., Oliveira, A.S., Brighente, I., Monteiro, F.B.F., Creczynski-Pasa, T.B., Szpoganicz, B., 2015. Preparation, characterization, cytotoxicity and antioxidant activity of DOPA melanin modified by amino acids: melanin-like oligomeric aggregates. J. Braz. Chem. Soc. 26, 273–281.

da Silva, T.U., Pougy, K. de C., Albuquerque, M.G., da Silva Lima, C.H., Machado, S. de P., 2022. Development of parameters compatible with the CHARMM36 force field for [Fe4S4] 2+ clusters and molecular dynamics simulations of adenosine-5'-phosphosulfate reductase in GROMACS 2019. J. Biomol. Struct. Dyn. 40, 3481–3491.

Daina, A., Michielin, O., Zoete, V., 2017. SwissADME: a free web tool to evaluate pharmacokinetics, drug-likeness and medicinal chemistry friendliness of small molecules. Sci. Rep. 7, 1–13.

Dallakyan, S., Olson, A.J., 2015. Chapter 19 Small-Molecule Library Screening by Docking with PyRx 1263, 243–250. https://doi.org/10.1007/978-1-4939-2269-7.

Durrant, J.D., McCammon, J.A., 2011. Molecular dynamics simulations and drug discovery. BMC Biol. 9, 1–9.

Ebanks, J.P., Wickett, R.R., Boissy, R.E., 2009. Mechanisms regulating skin pigmentation: the rise and fall of complexion coloration. Int. J. Mol. Sci. 10, 4066–4087.

Essmann, U., Perera, L., Berkowitz, M.L., Darden, T., Lee, H., Pedersen, L.G., 1995. A smooth particle mesh Ewald method. J. Chem. Phys. 103, 8577–8593.

Fan, R., Yuan, F., Wang, N., Gao, Y., Huang, Y., 2015. Extraction and analysis of antioxidant compounds from the residues of Asparagus officinalis L. J. Food Sci. Technol. 52, 2690–2700.

Galarce-Bustos, O., Pavón-Pérez, J., Henríquez-Aedo, K., Aranda, M., 2019. An improved method for a fast screening of α-glucosidase inhibitors in cherimoya fruit (Annona cherimola Mill.) applying effect-directed analysis via high-performance thin-layer chromatography-bioassay-mass spectrometry. J. Chromatogr. A 1608, 460415.

Haq, I., Imran, M., Nadeem, M., Tufail, T., Gondal, T.A., Mubarak, M.S., 2021. Piperine: A review of its biological effects. Phyther. Res. 35, 680–700.

Hess, B., Bekker, H., Berendsen, H.J.C., Fraaije, J.G.E.M., 1997. LINCS: a linear constraint solver for molecular simulations. J. Comput. Chem. 18, 1463–1472.

Huey, R., Morris, G.M., Forli, S., 2012. Using AutoDock 4 and AutoDock Vina with AutoDockTools : A Tutorial.

Irawan, C., Foliatini, H., 2017. GC-MS composition of leaf extract of Piper cf. arcuatum blume and their antioxidant activity and toxicity studies. J Pharmacogn Phytochem 6, 461–468.

Ismaya, W.T., Rozeboom, H.J., Weijn, A., Mes, J.J., Fusetti, F., Wichers, H.J., Dijkstra, B. W., 2011. Crystal structure of Agaricus bisporus mushroom tyrosinase: identity of the tetramer subunits and interaction with tropolone. Biochemistry 50, 5477–5486.

Jaisin, Y., Ratanachamnong, P., Wongsawatkul, O., Watthammawut, A., Malaniyom, K., Natewong, S., 2020. Antioxidant and anti-inflammatory effects of piperine on UV-B-irradiated human HaCaT keratinocyte cells. Life Sci. 263, 118607.

Karplus, M., McCammon, J.A., 2002. Molecular dynamics simulations of biomolecules. Nat. Struct. Biol. 9, 646–652.

Khan, Z., Hong, S.-M., Lee, J.-W., Moon, E.-Y., Huh, J., Chang, K.-A., Kim, S.Y., 2021. Potential of N-trans feruloyl tyramine from Lycium barbarum fruit extract on neurogenesis and neurotrophins; targeting TrkA/ERK/CREB signaling pathway. J. Funct. Foods 80, 104432.

Li, M., Li, T., Hu, X., Ren, G., Zhang, H., Wang, Z., Teng, Z., Wu, R., Wu, J., 2021. Structural, rheological properties and antioxidant activities of polysaccharides from mulberry fruits (Murus alba L.) based on different extraction techniques with superfine grinding pretreatment. Int. J. Biol. Macromol. 183, 1774–1783.

Lin, L.-C., Shen, C.-C., Shen, Y.-C., Tsai, T.-H., 2006. Anti-inflammatory Neolignans from Piper k adsura. J. Nat. Prod. 69, 842–844.

Liu, M.-Q., Li, J.-Y., Rehman, A.U., Xu, X., Gu, Z.-J., Wu, R.-C., 2019. Laboratory evolution of GH11 endoxylanase through DNA shuffling: effects of distal residue substitution on catalytic activity and active site architecture. Front. Bioeng. Biotechnol. 7, 350.

Mei, S., Chen, X., 2023. Combination of HPLC–orbitrap-MS/MS and network pharmacology to identify the anti-inflammatory phytochemicals in the coffee leaf extracts. Food Front.

Miller, M.A., Zachary, J.F., 2017. Mechanisms and morphology of cellular injury, adaptation, and death. Pathol. basis Vet. Dis. 2.

Moorthy, I.G., Maran, J.P., Muneeswari, S., Naganyashree, S., Shivamathi, C.S., 2015. Response surface optimization of ultrasound assisted extraction of pectin from pomegranate peel. Int. J. Biol. Macromol. 72, 1323–1328.

Mradula, P.R., Sacchidanand, S., 2012. A split-face comparative study of 70% trichloroacetic acid and 80% phenol spot peel in the treatment of freckles. J Cutan Aesthet Surg 5, 261.

Ngo, Q.M.T., Cao, T.Q., Hoang, L.S., Ha, M.T., Woo, M.H., Min, B.S., 2018. Cytotoxic activity of alkaloids from the fruits of Piper nigrum. Nat. Prod. Commun. 13, 1934578X1801301114.

Othman, A., Sayed, A.M., Amen, Y., Shimizu, K., 2022. Possible neuroprotective effects of amide alkaloids from Bassia indica and Agathophora alopecuroides: in vitro and in silico investigations. RSC Adv. 12, 18746–18758.

Pires, D.E.V., Blundell, T.L., Ascher, D.B., 2015. pkCSM: Predicting small-molecule pharmacokinetic and toxicity properties using graph-based signatures. J. Med. Chem. 58, 4066–4072. https://doi.org/10.1021/acs.jmedchem.5b00104.

Ramírez, D., Caballero, J., 2018. Is it reliable to take the molecular docking top scoring position as the best solution without considering available structural data? Molecules 23, 1038.

Safithri, Mega., Syaefudin, Weni, M., 2015. The Activity of Piper crocatum extract towards Inhibition of Tyrosinase activity and Malondialdehida Formation. Int. Semin. Sci. Complex Nat. Syst.

Safithri, M., Kurniawati, A., 2016. Formula of Piper crocatum, Cinnamomum burmanii, and Zingiber officinale extracts as a functional beverage for diabetics. Int. Food Res. J. 23, 1123.

Sedeky, A.S., Khalil, I.A., Hefnawy, A., El-Sherbiny, I.M., 2018. Development of core-shell nanocarrier system for augmenting piperine cytotoxic activity against human brain cancer cell line. Eur. J. Pharm. Sci. 118, 103–112.

Septiani, R., 2017. Ekstrak dan Fraksi Daun Sirih Merah (Piper crocatum Ruiz & Pav) sebagai Antioksidan dengan Metode 2, 2-difenil-1-pikrilhidrazil.

Sim, Y.Y., Ong, W.T.J., Nyam, K.L., 2019. Effect of various solvents on the pulsed ultrasonic assisted extraction of phenolic compounds from Hibiscus cannabinus L. leaves. Ind. Crop. Prod. 140, 111708.

Sneha, P., Doss, C.G.P., 2016. Molecular dynamics: new frontier in personalized medicine. Adv. Protein Chem. Struct. Biol. 102, 181–224.

Thiengsusuk, A., Muhamad, P., Chaijaroenkul, W., Na-Bangchang, K., 2018. Antimalarial activity of piperine. J. Trop. Med. 2018.

Tripathi, M.K., Ahmad, S., Tyagi, R., Dahiya, V., Yadav, M.K., 2022. Fundamentals of molecular modeling in drug design. In: Computer Aided Drug Design (CADD): From Ligand-Based Methods to Structure-Based Approaches. Elsevier, pp. 125–155.

Syaifie, P.H., Harisna, A.H., Nasution, M.A.F., Arda, A.G., Nugroho, D.W., Jauhar, M.M., Mardliyati, E., Maulana, N.N., Rochman, N.T., Noviyanto, A., Banegas-Luna, A.J., Pérez-Sánchez, H., 2022. Computational Study of Asian Propolis Compounds as Potential Anti-Type 2 Diabetes Mellitus Agents by Using Inverse Virtual Screening with the DIA-DB Web Server, Tanimoto Similarity Analysis, and Molecular Dynamic Simulation. Molecules 27, 3972. https://doi.org/10.3390/molecules27133972.

Vázquez-Martínez, J., Buitemea-Cantúa, G.V., Gutierrez-Villagomez, J.M., García-González, J.P., Ramírez-Chávez, E., Molina-Torres, J., 2020. Bioautography and GC-MS based identification of piperine and trichostachine as the active quorum quenching compounds in black pepper. Heliyon 6.

Vita, S.D., Chini, M.G., Bifulco, G., Lauro, G., 2021. Insights into the Ligand Binding to Bromodomain-Containing Protein 9 (BRD9): A Guide to the Selection of Potential Binders by Computational Methods. Molecules 26, 7192.

Wang, J., Wang, W., Kollman, P.A., Case, D.A., 2006. Automatic atom type and bond type perception in molecular mechanical calculations. J. Mol. Graph. Model. 25, 247–260.

Xu, Z., Chen, L., Jiang, M., Wang, Q., Zhang, C., Xiang, L.F., 2018. CCN1/Cyr61 stimulates melanogenesis through integrin α6β1, p38 MAPK, and ERK1/2 signaling pathways in human epidermal melanocytes. J, Invest. Dermatol. 138, 1825–1833.

Yu, Q., Fan, L., Duan, Z., 2019. Five individual polyphenols as tyrosinase inhibitors: Inhibitory activity, synergistic effect, action mechanism, and molecular docking. Food Chem. 297, 124910.

Zaelani, Bella Fatima Dora., Safithri, Mega., Adrianto, D., 2021. Molecular Docking of Red Betel (Piper crocatum Ruiz & Pav) Bioactive Compounds as HMG-CoA Reductase Inhibitor. J. Kim. Sains dan Apl. 24, 101–107.

Zaelani, B.F.D., n.d. Kajian In Silico dan In Vitro Piper crocatum Ruiz & Pav sebagai Inhibitor HMG-KoA Reduktase serta Aktivitas Penghambatan Terbentuknya Malondialdehida.

Zoete, V., Cuendet, M.A., Grosdidier, A., Michielin, O., 2011. SwissParam: a fast force field generation tool for small organic molecules. J. Comput. Chem. 32, 2359–2368.

Zolghadri, S., Bahrami, A., Hassan Khan, M.T., Munoz-Munoz, J., Garcia-Molina, F., Garcia-Canovas, F., Saboury, A.A., 2019. A comprehensive review on tyrosinase inhibitors. J. Enzyme Inhib. Med. Chem. 34, 279–309.